



RESEARCH ARTICLE

WILEY

Thermal sensor performance and fire characterisation during short duration engulfment tests

Shelley Kemp^{1,2} | Gary Proulx³ | Margaret Auerbach³ | Michael Grady³ | Roger Parry⁴ | Martin Camenzind¹

¹Laboratory for Biomimetic Membranes and Textiles, Empa, Swiss Federal Laboratories for Materials Science and Technology, St. Gallen, Switzerland

²Centre for Materials Innovation and Future Fashion, School of Fashion and Textiles, RMIT University, Melbourne, Australia

³U.S. Army Natick Soldier Research, Development and Engineering Center, Natick, MA, USA

⁴DuPont Protection Solutions, Richmond, VA, USA

Correspondence

Martin Camenzind, Laboratory for Biomimetic Membranes and Textiles, Empa, Swiss Federal Laboratories for Materials Science and Technology, Lerchenfeldstrasse 5, 9014 St. Gallen, Switzerland.

Email: martin.camenzind@empa.ch

Summary

A small-scale reproduction of the ISO 13506-1 thermal manikin was constructed to enable the assessment of manikin sensor performance, the partitioning of energy, and the variability of the fire generated during short duration heat and flame engulfment tests. The cylindrical test apparatus simultaneously housed four total heat flux (THF) sensors, one radiant heat flux sensor, and three manikin sensors. Calibrated manikin sensors were provided by nine laboratories and were categorised as buried thermocouple, copper-based, or surface-mounted thermocouple sensors. The test apparatus was exposed to fire generated by four propane torches for three exposure durations. All sensors presented similar profiles in net heat flux over time, which could be divided into four distinct phases: transient increase, pseudo-steady state, transient decrease, and post-exposure. Over pseudo-steady state, the mean THF over all exposure durations was $88 \pm 8 \text{ kW/m}^2$, and the ratio of convective to radiant energy was approximately 50:50, but highly variable. For a 4-second exposure, manikin sensors from five laboratories had a bias in heat flux greater than $\pm 5\%$ during pseudo-steady state when compared with the THF sensors. This bias can primarily be attributed to the sensitivity of the manikin sensors to convective heat or heat loss due to sensor design.

KEY WORDS

calibration, convection, manikin, Protective clothing against heat and flame, radiation, sensor

1 | INTRODUCTION

Thermal manikins are used to evaluate the performance of complete garments exposed to short duration heat and flame engulfment.¹ Sensors embedded within the manikins' surface (manikin sensors) record the change in heat flux directly or enable the calculation of heat flux through transient changes in temperature. From heat flux, the energy transferred through the test garment over a defined time period (ISO 13506-1), and the predicted skin burn injury (ISO 13506-2) are calculated.^{1,2} The manikin sensors are expected to respond to the full range of heat fluxes (approximately 0–130 kW/m^2)

and heat transfer modes which may be encountered during tests. Heat and flame engulfment is calibrated by exposing the nude manikin (without garment) to a mean incident heat flux of $84 \text{ kW/m}^2 \pm 5\%$ across all sensors over the period of pseudo-steady state* (here forth referred to as manikin exposure calibration). The heat fluxes recorded under a garment are typically much lower than those encountered during manikin exposure calibration, and are influenced by garment composition and design, and exposure duration (3–12 s).

*The ISO 13506-1:2017 standard currently defines pseudo-steady state as the 'steady region' of the heat flux curve.

ISO 13506-1:2017 stipulates that the manikin sensors shall be calibrated using a single-mode radiant energy source between 8 kW/m^2 and 30 kW/m^2 against a certified total heat flux (THF) reference sensor such as the Schmidt-Boelter or Gardon-Gauge.¹ There are advantages and disadvantages with the specified method of calibration. Radiant heat is a reproducible heat source and is typically used for the calibration of THF reference sensors.³ However, a single-mode energy source is not representative of the mixed-mode energy encountered during the short duration heat and flame engulfment tests defined by ISO 13506-1. Additionally, the calibration range specified is 1) less than the range over which the manikin sensors are expected to perform, and 2) does not cover the entire range of heat fluxes used in the calculation of predicted skin burn injury, which is based on the work of Stoll and Greene.^{2,4}

There are a number of manikin sensor technologies which currently meet the requirements of ISO 13506-1:2017. In 2016, twelve laboratories participated in an ISO 13506 round robin.⁵ The sensors used by participating laboratories varied in size, composition, and design, but could be broadly categorised into three sensor families. Six laboratories used a *buried thermocouple sensor*, where the thermocouple is embedded in epoxy or 'ceramic'. Four laboratories used a *copper-based sensor*, which contains a copper slug (typically insulated by a copper guard) and a rear mounted thermocouple. The remaining two laboratories used a *surface-mounted thermocouple sensor*, where the thermocouple is adhered to the outer surface of a 'skin simulant' sensor.

Manikin sensor technologies have previously been compared in both experimental and theoretical research.^{6,7} The performance of three manikin sensors (a buried thermocouple sensor, an insulated copper-based sensor, and a surface-mounted thermocouple sensor) were compared to the performance of the ISO 9151 copper disc calorimeter, a commonly available temperature sensor.⁸ The sensors were exposed to three nude exposure conditions (radiant heat $\sim 6 \text{ kW/m}^2$, radiant heat $\sim 12 \text{ kW/m}^2$, and 50/50 radiant/convective heat $\sim 84 \text{ kW/m}^2$) and one garment exposure condition ($\sim 84 \text{ kW/m}^2$, 3 fabrics, 6 mm air gap).⁶ The researchers concluded that the insulated copper-based sensor responded in a manner similar to the ISO 9151 copper disc calorimeter. This result is not surprising given that the insulated copper-based sensor and the ISO 9151 copper disc calorimeter are similar in composition and construction, and are therefore susceptible to the similar heat losses and decay processes.⁹ Furthermore, the sources of the heat and flame (quartz tubes and ISO 9151 gas burners) were not equivalent to the heat and flame encountered during short duration engulfment tests. The constructional features, working principles, and sensor characteristics of the ISO 9151 copper disc calorimeter, the buried thermocouple sensor, the copper-based sensor, the surface-mounted thermocouple sensor, and THF reference sensors (Schmidt-Boelter, Gardon-Gauge) have been discussed by Mandal and Song (2014). However, due to the limited information available in the public domain this review of literature does not adequately cover the complexities of each sensor technology.⁷

During a nude exposure, the manikin sensors are exposed to mixed-mode heat transfer, which is a combination of radiant heat transfer (the transmission of energy by electromagnetic waves) and

convective heat transfer (energy transfer by means of fluid motion). The exact partitioning of the energy among these modes of heat transfer during short duration heat and flame engulfment tests is unknown. It is important to understand how each manikin sensor technology responds to mixed-mode heat transfer when calibrated using radiant only heat. Fundamentally, the sensors must perform comparability in order to achieve reproducible conditions during manikin exposure calibration and reproducible results for garment tests.

ISO13506-1:2017 is an extremely complex test method, and therefore inter- and intra-laboratory variation is expected. However, the magnitude of variation in the inter-laboratory test data reported in ISO 13506-1:2017 Annex B is unacceptable to the end user.^{1,5} The ISO 13506 round robin identified manikin sensor performance and sensor calibration as key factors in improving the reproducibility of the ISO 13506 test standard.⁵

The current work had three objectives: 1) to compare the performance of manikin sensor technologies during short duration heat and flame engulfment tests similar to those defined by ISO 13506-1, 2) to characterise the fire generated during such tests by assessing the stability, repeatability, and the partitioning of the convective and radiative energy, and 3) to investigate the use of an instrumented test cylinder as an alternative method for the calibration of manikin sensors.

2 | METHOD

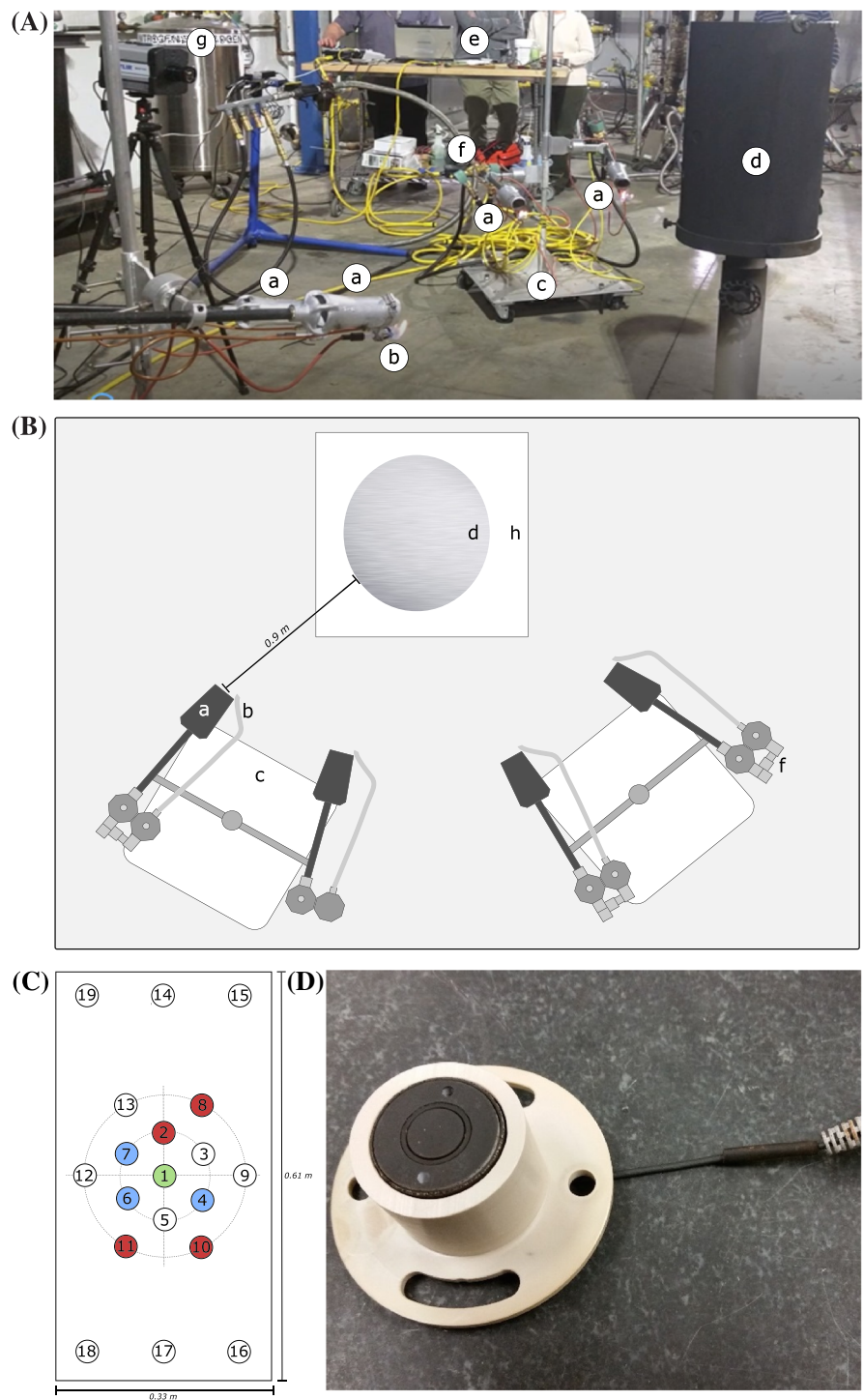
2.1 | Test apparatus

The instrumented test cylinder (Figure 1A–D) was constructed by the US Army Natick Soldier Research, Development and Engineering Center. The cylindrical shape and size (0.33 m diameter, 0.61 m in length) were selected to approximate that of an average human torso and to minimize stagnation of the flames. The cylinder was fabricated from a preformed tube of Norplex-Micarta RT310. The tube was populated with 19 holes (35 mm in diameter) for sensor mounting and coated with a thin layer of black high-temperature paint (Zynolyte Hi-Temp Extreme Heat Enamel, absorptivity > 0.9). Circular adapters, fabricated from polyether ether ketone (TECAPEEK 450G), were custom-made allowing all sensors to be mounted flush with the surface of the cylinder (Figure 1D). Sensors were spaced as close as possible while accommodating the mounting of adapters (approximately 75 mm between each sensor).

For each test, nine sensors were mounted on the face of the cylinder: one radiant heat flux (RHF) sensor in position 1, four total heat flux (THF) sensors in positions 2, 8, 10, and 11, and three manikin sensors in positions 4, 6, and 7 (Figure 1C). The nine sensors were arranged in two rings around a central position (position 1). Unused sensor mounts were sealed during testing. Sensor positions were selected based on the heat distribution encountered during pretesting.

Four Bertha L. B White 500 K propane torches (diameter ~ 97 mm, nozzle mixing, trust-driven, with orifices removed) compliant with ISO13506-1:2017 were mounted on two stands (Figure 1A and B). The torches were positioned ~ 0.9 m from the

FIGURE 1 Test apparatus A, photograph of the test setup, B, two-dimensional schematic of the torch and cylinder configuration, C, two-dimensional schematic of the test cylinder indicating sensor positions (1, RHF sensor; 2, 8, 10, and 11: THF sensors; 4, 6, and 7, manikin sensors; 3, 5, 9, 12-19, unused positions), and D, a typical example of a manikin sensor in sensor mount. Key: a. torch, b. pilot torch, c. torch stand, d. test cylinder, e. data acquisition, f. gas supply, g. FLIR camera, h. cylinder stand)



¹RdF Corporation. 22 Elm Avenue, Hudson, 03051, USA. www.rdfcorp.com

²THF sensor: Calorimeter, water cooled. RdF Microfoil[®]. Output: 1 mV per BTU/Ft²/sec. Standard calibrated range: 0 - 30 BTU/Ft²/sec, over range capability to 30 BTU/Ft²/sec.

Housing body operating temperature: -50 to 200°F. Impedance: 200 Ohm maximum.

Response time: 16 ms nominal. Recommended water cooling 0.25 GPM. Sensing area 0.25 x 0.26 inch. Sensing surface: hard 'black' anodised aluminium.

³RHF sensor: Fast response radiometer with transparent window. Output: 0 - 40 ± 10 mV. Range: 0 - 35 BTU/Ft²/sec. Temperature range -300 to 500°F. Impedance: 200 Ohm maximum. Response time: 10 ms nominal. Sensing area ø 0.500 inch. Sensing surface: fibrous phenolic thermal insulator.

surface of the cylinder. Torches 1 and 4 and torches 2 and 3 were at an approximate height of 0.86 m and 0.69 m, respectively. The torches were angled towards the base of the cylinder (~0.81 m high) to account for the upward movement of the heat and flame. During pretesting this configuration generated similar heat flux values across the four THF sensors and produced flames which visually resembled those encountered during ISO 13506-1 manikin exposures. An infrared camera (FLIR, SC6700 IR camera with a 13 mm lens and a portable data recorder) was used to assess the distribution of heat across the surface of the cylinder prior to and following the exposures. Priority

was placed on achieving an even distribution of the heat across the sensors rather than on a specific absolute heat flux. Residential grade propane (HD-5) compliant with ISO 9162 was used.¹⁰

2.2 | Sensors

The THF was measured using four water-cooled, traceable, commercial reference heat flux sensors from RdF Corporation[†] (model 27650-20-120[‡]). This sensor operates on the principles of a Schmidt-Boelter sensor but has a thermopile (Microfoil[®]) for improved response times (16 ms). Such sensors register the cold wall heat flux and are sensitive to both radiation and convection.^{3,11} Note that the cold-wall heat flux measured by the THF sensors is greater than that measured by a hot-wall sensor, given the same boundary conditions.¹² A Cole Palmer Polystat Advanced 8.6 L Heat/Cool Bath was used to maintain the temperature of the water supplied to the THF sensors. The surface absorptivity of the THF sensors to radiant energy was ~0.9. The RHF was measured using a RdF Corporation radiometer (model 27714[§]), which is sensitive only to radiant heat. The RHF sensor was not water cooled. The THF and RHF sensors were calibrated by RdF Corporation to net (absorbed) heat flux using a NIST traceable radiant only energy source (calibration range: 0–230 kW/m²). Sensitivity to convection was not provided by the manufacturer, and thus the assumption was made that the response is linear. When used in a mixed radiative-convective environment, the uncertainties in the measured THF are higher than those listed by the manufacturer.¹³ The performance of the THF and RHF sensors were assessed prior to and after the experimental work; no significant changes in performance were observed.

Each of the nine participating laboratories provided three calibrated manikin sensors (Table 1). The manikin sensors were calibrated by the laboratories according to ISO 13506-1:2017, that is, with a primarily radiant heat source between 8–30 kW/m² (Table 2). Five laboratories used buried thermocouple sensors (four in epoxy, one in ‘ceramic’), three used copper-based sensors, and one used a surface-mounted thermocouple sensor. The sensors were manufactured by Precision Products, Thermetrics, Okazaki Manufacturing Company, or in-house. None of the manikin sensors were water cooled. All of the manikin sensors gave a data output in temperature, which was then converted to heat flux (Table 3; Section 2.4). Schematics of common sensors technologies are available in Song et al., 2017.¹⁴ The thermal properties of the sensor materials are presented in Table 4.

2.3 | Test method

For each test, three manikin sensors from the same laboratory, four THF sensors, and one radiant heat flux sensor were mounted in the cylinder and subjected to heat and flame engulfment. The tests were repeated for the manikin sensors from all nine laboratories, and for three exposure durations (3, 4, and 5 s). Each variant was tested in triplicate. For logistical reasons, the test order was grouped by manikin

sensors and by burn duration. Between exposures, all sensors were cooled to less than 38°C in accordance with ISO 13506-1, as verified by sensor temperature readings and the FLIR camera. All sensors were cleaned with an alcohol wipe between each test and allowed it to dry as the cylinder/sensors cooled.

Over the duration of the tests, the mean air temperature (\pm standard deviation) was $22.5 \pm 1.8^\circ\text{C}$, the relative humidity was $49.4 \pm 3.9\%$, the coolant water temperature was $32.2 \pm 0.6^\circ\text{C}$, and the coolant flow was $1.15 \pm 0.1 \text{ l/m}$. The test chamber has a volume of $\sim 1200 \text{ m}^3$ and is 50 m above sea level.

2.4 | Data acquisition

Temperature and heat flux data were recorded using a National Instruments SCXI-1600, USB 16-bit Digitizer Module with a SCXI-1102 Signal Conditioning Module and a SCXI-1303 Isothermal Terminal Block, at a frequency of 10 Hz (resolution for T- and K-type thermocouples is 0.1°C ($\sim 4 \mu\text{V}$), or better). Data acquisition began approximately 3 s prior to exposure and recorded for a total duration of 60 s.

The temperature data from the manikin sensors were provided to each laboratory who converted temperature to net heat flux (q_{net}) using the calibration factors generated prior to testing. ISO 13506-1:2017 states that heat flux should be calculated ‘using the appropriate technique for the sensor being applied’. A brief description of how this is done by each laboratory is provided in Table 3. Simply stated, the net heat flux is the amount of energy registered by the sensor (this has historically, but incorrectly, been referred to as the absorbed heat flux). The incident heat flux is the amount of energy impinging on the system. Unless otherwise specified, from here forth ‘heat flux’ refers always to the net heat flux (without mathematical corrections for post-exposure offset, convective heat transfer, or heat losses). Little guidance is given by the standard in regard to what post-processing is and is not acceptable. Nonparametric spline smoothing and median filters, for example, are reportedly used by laboratories to reduce noise and remove erroneous spikes in the heat flux data. The amount of post-processing (filtering and smoothing) applied by laboratories to the data was not stipulated. For the THF or RHF sensor data, no post-processing was conducted. The laboratories were blinded to the other test data. The data was compiled and analysed by a single laboratory.

2.5 | Calculation of heat flux, TE, and offset

For each sensor type, the following parameters were quantified (Figure 2).

- Start and end of exposure(s)
The start and end of exposure were defined as the time point at which heat flux reached 20% of its maximum value.
- Mean heat flux and the deviation in heat flux over pseudo-steady state (kW/m²)

TABLE 1 Manikin sensor specifications for each of the participating laboratories

Manikin sensor family	Laboratory	Manikin sensor type	Sensor diameter	Sensor length	Thermocouple size	Surface of sensor ^a	Surface emissivity
Buried thermocouple sensor	Lab 1	T-type thermocouple (copper/constantan) buried in epoxy resin at a depth of ~ 0.3 mm (4xxx series)	27 mm	28 mm	0.1 mm	Teflon surface coated with Krylon 4290 ultra-flat black paint	~ 0.97
	Lab 2	T-type thermocouple buried in epoxy resin at a depth of ~ 0.3 mm (7xxx series)	27 mm	28 mm	0.1 mm	Teflon surface coated with Krylon 4290 ultra-flat black paint	~ 0.97
	Lab 3	T-type thermocouple buried in epoxy resin at a depth of ~ 0.3 mm (8xxx series)	27 mm	28 mm	0.1 mm	Teflon surface coated with Krylon 4290 ultra-flat black paint	~ 0.97
	Lab 4	T-type thermocouple buried in epoxy resin at a depth of ~ 0.3 mm (5xxx series)	27 mm	28 mm	0.1 mm	Teflon surface coated with Krylon 4290 ultra-flat black paint	~ 0.97
	Lab 5	K-type thermocouple (nickel-chromium/nickel-alumel) buried in a 'ceramic' composite of glass fibre, boron, and epoxy resin. Depth of thermocouple not available.	24 mm	35 mm	0.2 mm	Ichinen Tasco Co. Ltd. black paint (TA410KS)	~ 0.94
Surface-mounted thermocouple sensor	Lab 6	T-type thermocouple adhered to the surface of colorceran using epoxy-phenolic adhesive.	19 mm	32 mm	~ 0.1 mm (rolled flat)	Krylon High Heat (#1618)	~ 0.9
Copper-based sensor	Lab 7	guarded copper slug with a T-type thermocouple, mounted in Macor ceramic	slug: 11.2 mm guard: 13.7 mm	slug: 1.5 mm guard: 2.0 mm	0.5 mm	Medtherm Corp flat black paint	~ 0.95
	Lab 8	guarded copper slug with T-type thermocouple	mount: 23 mm slug: 11 mm guard: 25 mm	mount: 13 mm slug: 1.5 mm guard: 27 mm	0.4 mm	Zynolyte Z635 Quick Dry Hi-Temp Black Paint	~ 0.95
	Lab 9	guarded copper slug with a T-type thermocouple	slug 13 mm guard: 26 mm	slug: 1.5 mm guard: 27 mm	0.3 mm	Medtherm Corp flat black paint	~ 0.95

Note. ISO 13506 states that 'The outer surface of the sensor shall have an absorptivity greater than or equal to 0.9 or shall be covered with a thin layer of flat black high-temperature paint with an absorptivity greater than or equal to 0.9'. The emissivity of the epidermis of human skin is reportedly 0.98.¹⁵

TABLE 2 Manikin sensor calibration procedure for each of the participating laboratories^{16,17}

Manikin sensor family	Laboratory	Calibration apparatus	Total heat flux reference sensor	THF sensor adjacent	Duration of exposure	Definition of pseudo-steady state	Target heat flux used for calibration
Buried thermocouple sensor	Lab 1	ISO 6942 apparatus ¹⁶	Schmidt-Boelter - Medtherm 64 series	yes	10 s	2 s offset from start and finish, detected as 75% of max value	8, 15, & 30 kW/m ²
	Lab 2	gas fired radiant heat	Schmidt-Boelter - Medtherm	yes	10 s	2 s offset from start and finish, detected as 75% of max value	25 kW/m ²
Lab 3	gas fired radiant heat	Gardon guage -Vatell		yes	14 s	from 2 to 12 s	20 kW/m ²
Lab 4	ISO 6942 apparatus	Schmidt-Boelter - Medtherm 64 series		yes	10 s	2 s offset from start and finish, detected as 75% of max value	8, 15, & 30 kW/m ²
Lab 5	ISO 6942 apparatus	Schmidt-Boelter - Medtherm (24-10FSB-16-21054K)		no	10 s	from 1 to 9 s	8, 15, & 30 kW/m ²
Surface-mounted thermocouple sensor	Lab 6	handheld lamp	Schmidt-Boelter - Medtherm 64 series		9 s	last 3 s of the exposure	8-16 kW/m ²
Copper-based sensor	Lab 7	a) ISO 6942 apparatus b) handheld radiant lamp	Schmidt-Boelter -Hukseflux SBG01-200	a) yes, b) no	15 s	2 s offset from rising edge and falling edge	30 & 60 kW/m ²
	Lab 8	gas fired radiant heat	Schmidt-Boelter - Medtherm	yes	10 s for low fluxes & 4 s for high fluxes	based on dq/dt of the THF sensor	10, 45, & 90 kW/m ²
	Lab 9	ASTM F1939 apparatus ¹⁷	Schmidt-Boelter -Medtherm 64 series	no	10 s	0.5 s after the start to the finish	12 kW/m ²

TABLE 3 Calculation of net heat flux from temperature as conducted by each of the participating laboratories

Manikin sensor family	Laboratory	Conversion of temperature to net heat flux
Buried thermocouple sensor	Labs 1-4	<p>In brief, heat flux is calculated as follows.</p> $\frac{\partial T(x,t)}{\partial t} = \frac{k}{\rho C_p} \frac{\partial^2 T(x,t)}{\partial x^2}$ <p>The time/temperature data is used to calculate the direct part of the sensor internal temperature field problem (from the thermocouple to the isothermal backwall).</p> $\frac{T_i^{n+1} - T_i^n}{\Delta t} = \frac{k(T_i^n)}{2\rho C_p(T_i^n)} \left[\frac{T_{i-1}^{n+1} - 2T_i^{n+1} + T_{i+1}^{n+1}}{(\Delta x)^2} + \frac{T_{i-1}^n - 2T_i^n + T_{i+1}^n}{(\Delta x)^2} \right]$ <p>A time and space marching technique of Raynaud & Bransier¹⁸ is used to solve the inverse part of the problem (IHCP1D, thermocouple to the surface).</p> <p>With all the i-2 nodes determined, the sensor surface heat flux is then calculated from the equation below, which is the finite approximation of the energy balance equation for the boundary surface:</p> $q_{i-2}^{n+1} = k(T_{i-2}^{n+1}) \frac{T_{i-2}^{n+1} - T_{i-1}^{n+1}}{\Delta x} + \rho C_p(T_{i-2}^{n+1}) \frac{T_{i-2}^{n+1} - T_{i-2}^n}{\Delta t} \frac{\Delta x}{2}$
	Lab 5	<p>Heat flux calculated according to Crown and Dale, 1992¹⁹</p> $q(t) = \sqrt{\frac{k\rho C_p}{\pi}} \left[\frac{1}{2} \int_0^t \frac{T_s(\tau) - T_i(\tau)}{(t-\tau)^{3/2}} d\tau + \frac{T_s(t) - T_i}{t^{1/2}} \right]$ <p>Where: q(t) is the heat flux (W/m²) at time t, k is thermal conductivity (W/mk), ρ is density (kg/m³), Cp is thermal capacity (J/kgK), Ts(t) is surface temperature of sensor (K), t is lapsed time (second), and Ti is surface initial temperature of sensor (K).</p>
Surface-mounted thermocouple sensor	Lab 6	$q''(t) = \sqrt{\frac{k\rho C_p}{\pi}} \left[\frac{1}{2} \int_0^t \frac{T_s(\tau) - T_i}{t^{1/2}} d\tau \right]$ <p>Where: q''(t) is the heat flux (W/m²) at time t, k is thermal conductivity (W/mk), ρ is density (kg/m³), Cp is thermal capacity (J/kgK), Ts(t) is surface temperature of sensor (K), t is lapsed time (second), and Ti is surface initial temperature of sensor (K).</p>
Copper-based sensor	Lab 7	$q(t) = q_A(t) + q_B(t)$ $q_A(t) = \text{CalA} \cdot C_p(t) \cdot \left(\frac{dT(t)}{dt} \right)$ $q_B(t) = \text{CalB} \cdot (T(t) - T_{internal}(t))$ $T_{internal}(t) = T_{internal}(t_{n-1}) + \text{CalC} \cdot q_B(t_{n-1}) \cdot dt$ <p>Where: q(t) is the heat flux (W/m²) at time t (seconds) comprised of two components q_A(t) and q_B(t), T(t) is measured temperature of sensor (C), C_p(t) is thermal capacity (J/gC) computed at actual sensor temperature, CalA, CalB, and CalC are calibration parameters for the sensor, and T_{internal}(t) is a virtual predicted internal sensor temperature.</p>
	Lab 8	$q = C1 \frac{dT(t)}{dt} + C2(T(t) - T_b)$ <p>C1 is dependent on density, thermal conductivity, and effective thickness.</p> <p>C2 is dependent on mounting body characteristics</p> <p>C1 and C2 are empirically fit.</p> <p>Tb is the lumped body temperature used to calculate losses</p> $Tb_i = \epsilon(T_i - Tb_{i-1}) + Tb_{i-1}$ <p>Where:</p> $\eta = \frac{0.5}{\sqrt{dt}}$ $\epsilon = erfc(\eta)$
	Lab 9	$q = \rho C_p C_L \frac{dT(t)}{dt} + K_L(T(t) - T_i)$ <p>Where: ρ is the density of copper, Cp is the specific heat of copper, C_L is the copper disc thickness factor (determined experimentally), L is the thickness of the copper slug, T(t) is the temperature of the copper slug at a specific time, t is time, K_L is the aggregate contact conductance between the copper disc and the supporting insulator (determined experimentally).</p>

Note. The information provided by the laboratories (through personal communications) is a brief summary of the methods used to determine heat flux, not a comprehensive guide for each sensor technology. References have not been included to maintain anonymity. Unless otherwise specified the calibration factor for the manikin sensor in question is subsequently applied to the heat flux data.

Pseudo-steady state was defined as beginning 1.5 s after the start of exposure and ending 0.5 s before the end of the exposure. This definition was based on what is currently used by the laboratories during calibration (Table 2) and on preliminary test data; the definition was agreed upon by all participating laboratories. For each test, the mean heat flux from the manikin sensors (n = 3) and the mean heat flux from the THF sensors (n = 4) was calculated.

- Transferred energy per unit area (TE; kJ/m²)
- TE was calculated, according to Equation (Eq 1), at two time points: TE_{end} (TE at the end of the exposure to heat and flame, i.e. after 3, 4, or 5 s) and TE₃₀ (TE 30 s after the start of the exposure).²⁴ For both calculations, TE included a 1 s baseline of data prior to the start of exposure (TE₋₁). TE is the integral of the net heat flux over the calculation period and is thus uncorrected for convective heat transfer.

TABLE 4 Thermal properties of sensors materials

Primary material component of sensor	Thermal conductivity [W/(mK)]	Volumetric heat capacity [J/(m ³ K)]	Thermal diffusivity [m ² /s]	Thermal inertia, kpc [J ² /m ⁴ .K ² .s]
<i>Copper-based sensor</i>				
copper ^a	400	3.5E+06	1.2E-04	1.4E+09
<i>Buried thermocouple sensor</i>				
epoxy resin ^a	0.29	2.2E+06	1.3E-07	6.4E+05
ceramic (glass fibre, boron, and epoxy resin) ^a	0.30	2.4E+06	1.2E-07	7.3E+05
<i>Surface-mounted thermocouple sensor</i>				
colorceran ^a	0.97	1.7E+06	5.7E-07	1.6E+06
<i>Human tissue^b</i>				
epidermis	0.63	4.4E+06	1.4E-07	2.7E+06
dermis	0.58	4.2E+06	1.4E-07	2.2E+06
sub-cutaneous	0.29	2.6E+06	1.1E-07	7.9E+06

Roger Parry, PhD., email communication, August 16, 2018, Doug Dale, PhD., email communication, August 16 2018, 2,4,²⁰⁻²³

Note 1: Unless reported otherwise, the volumetric heat capacity was calculated as the specific heat capacity multiplied by the density; the thermal diffusivity was calculated as the thermal conductivity divided by the volumetric heat capacity, and the thermal inertia was calculated as the thermal conductivity multiplied by the density and the specific heat capacity.

^athermal properties reported at 25°C

^bISO 13506-2 physical properties for the skin model with thermal conductivity independent from temperature (skin model B).

- Offset (kW/m²)

Offset in heat flux following exposure was averaged over a 20 s time period, beginning 5 s after the end of the exposure (as indicated by the mean end time of THF sensors).

$$q_i = \sum_0^t q_i(t) \cdot \Delta t \quad (\text{Eq1})$$

Where: q_i is the transferred energy of sensor i in J/m², $q'_i(t)$ is the heat flux of sensor i at time t in W/m².

From the mean heat flux during pseudo-steady state, the partitioning of radiant and convective energy and manikin sensor bias was determined. The partitioning of the mixed-mode heat was established by comparing the RHF and THF responses, with the difference between the RHF and THF attributed to convective energy. Sensor bias was calculated as the manikin sensor response expressed as a percentage of the mean of the THF sensors. Sensor bias in TE was calculated in the same manner.

2.6 | Statistical analyses

Descriptive and inferential statistics were generated using Microsoft Excel and SPSS statistical software (SPSS version 22; IBM). Unless otherwise stated, the results are reported as means \pm standard deviations (coefficient of variation, CV). The effect of exposure duration on RHF, THF, and the partitioning of radiant heat was determined using a one-way ANOVA. Normality was assessed for all parameters using the Shapiro-Wilk test. Levene's tests were used to verify the equality

of variance. For all tests, statistical significance was set at $\alpha = 0.05$. During the first test session a fault was noted in the RHF sensor performance. The RHF sensor was replaced and the RHF data from six tests excluded from analysis.

3 | RESULTS

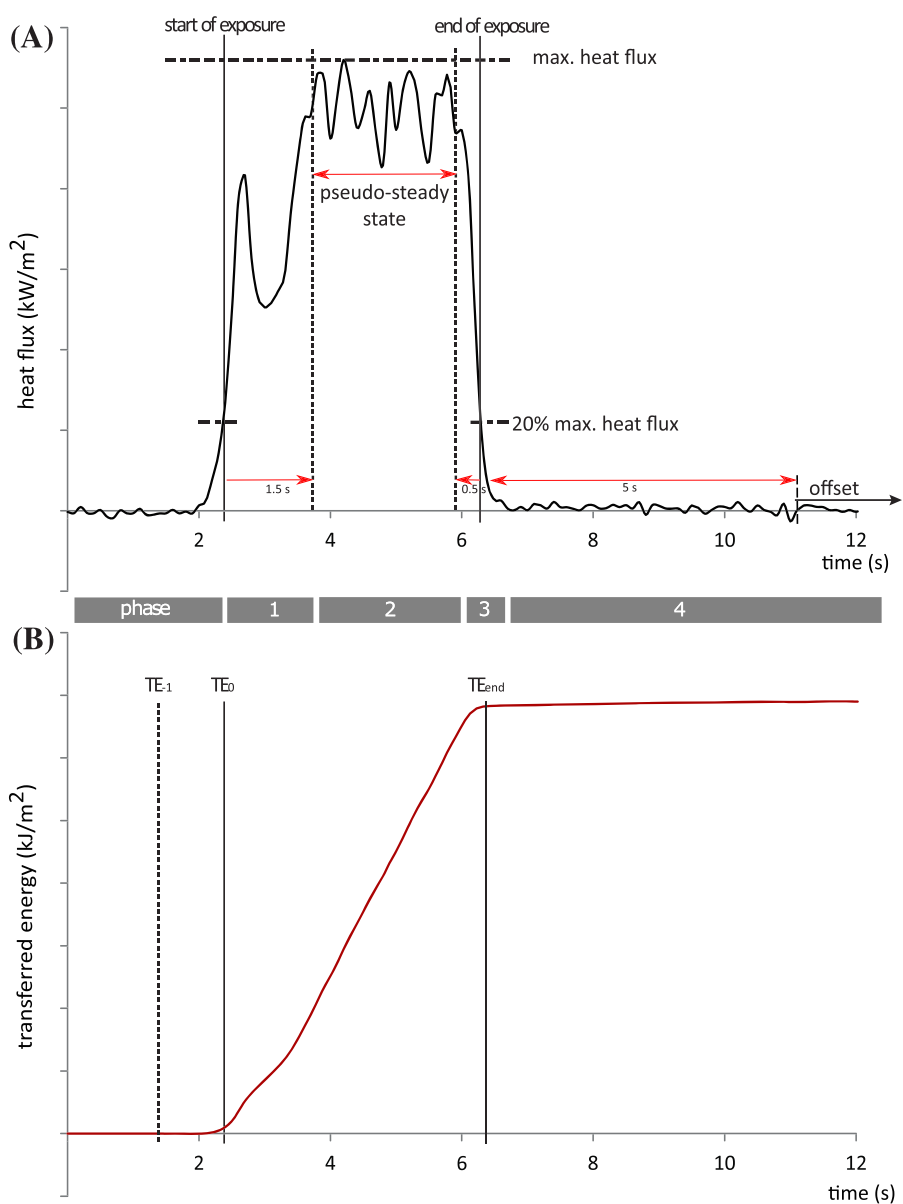
For all sensor types the heat flux trace over time can be divided into four distinct phases:

- Phase 1—transient increase: the transient phase during the first ~1.5 s of the exposure where the heat flux increases in response to the heat and flame. The initial increase in heat flux was invariably followed by a dip, and then a second rise to the period of pseudo-steady state.
- Phase 2—pseudo-steady state: a period of relatively stable heat flux.
- Phase 3—transient decrease: the transient phase during the last ~0.5 s of the heat flux curve (the period immediately following the end of exposure) where heat flux decreases.
- Phase 4—post-exposure: the phase following exposure, in which an offset in heat flux may be observed (Figure 2, Appendix 1).

3.1 | Radiant heat flux (RHF)

The mean RHF during pseudo-steady state was 43.0 ± 5.2 kW/m² (12.1%), which equates to $48.5 \pm 4.1\%$ of the total heat flux. The

FIGURE 2 Test outputs A, heat flux curve over time and B, TE curve over time



remaining 51.5% was attributed to convective heat transfer. Exposure duration did not have a significant effect on the absolute radiant heat flux ($F_{2,73} = 1.463, p = 0.238$) or the proportion of radiant heat ($F_{2,73} = 2.686, p < 0.075$).

3.2 | Total heat flux (THF)

Across all exposures, the mean THF during pseudo-steady state was 87.7 kW/m². The inter-test variation (the standard deviation in the mean total heat flux across all exposures during pseudo-steady state, i.e. the repeatability) was ± 7.7 kW/m² (8.7%). Exposure duration did not influence heat flux during pseudo-steady state ($F_{2,80} = 0.333, p = 0.718$). The mean intra-test variation (standard deviation of the four THF sensors within a single exposure, which is a measure of the heat distribution across the cylinder during pseudo-steady state) was ± 4.6 kW/m², ± 3.6 kW/m², and ± 3.4 kW/m², for 3, 4, and

5-second exposures respectively (Appendix 2, Table A2.1). The mean standard deviation over the duration of pseudo-steady state (an indicator of the heat stability) was ± 11 kW/m² (13%). Given the variation in the magnitude of THF among exposures, the manikin sensor responses were expressed as a percentage of the mean THF of the same exposure.

3.3 | Manikin sensors

3.3.1 | Profiles

The heat flux profiles over time for all manikin sensors were similar to the THF sensor profiles (Appendix 1). For the manikin sensors, the magnitude of the fluctuations in heat flux over the duration of the exposure varied in comparison to the THF sensors. For the manikin sensors, the post-processing of data (smoothing and

filtering) was not restricted, the standard deviation over the period of pseudo-steady state was therefore not assessed. Two manikin sensors (one each from Labs 4 and 5) were excluded from analysis. Visual analysis of the heat flux curves and the intra-test variation indicated that the sensors were faulty or erroneously calibrated (Appendix 2). For Lab 4, the exclusion of the single sensor resulted in a considerable reduction in the intra-test variation (Appendix 2, Table A2.1). However, for Lab 5 the intra-test variation remained high even with the exclusion of a single sensor, and thus this data shall be interpreted with caution.

3.3.2 | Heat flux over pseudo-steady state

Sensor bias over pseudo-steady state varied among the manikin sensors and exposure durations (Figure 3). Taking the 4-second exposures as an example, the manikin sensors from five of the nine laboratories (Labs 2, 3, 4, 5, and 8) were beyond $\pm 5\%$ of the mean THF. A deviation of 5% was deemed to be a relevant bias, as it is the equivalent of the deviation accepted during manikin exposure calibration. The greatest bias in heat flux was typically observed for the 3-second exposures. For the manikin sensors from Labs 1, 7, and 9 the mean bias was within $\pm 5\%$ for all exposure durations. Lab 9 showed the least inter-test variation in bias. Labs 4, 5 and 7 showed the greatest inter-test variation in bias (Figure 3).

3.3.3 | Offset

For the 4-second exposures, the manikin sensors from two laboratories (Labs 8 and 9) had a negative offset greater than 5 kW/m^2 . Manikin sensors from two laboratories (Labs 5 and 6) had a positive offset greater than 0.5 kW/m^2 . The manikin sensors from the remaining laboratories were within $\pm 0.5\text{ kW/m}^2$. For those

sensors with significant offsets, the magnitude appeared to be influenced by the exposure duration, with longer exposure durations having greater offsets (Table 5). For the THF sensors the mean offset was less than 0.2 kW/m^2 .

3.3.4 | Transferred energy

For the 4-second exposures, bias at TE_{end} was less than 5% for the manikin sensors from only two laboratories (Labs 1 and 9; Figure 4). The bias at TE_{30} was less than 5% for the manikin sensors from three laboratories (Labs 1, 2, and 3). The remaining laboratories' sensors had biases at TE_{30} greater than 5% (Lab 4: -8%, Lab 5: 8%, Lab 6: 10%, Lab 7: 11%, Lab 8: -46% and Lab 9: -48%). The bias increased considerably between TE_{end} and TE_{30} for manikin sensors that had an offset in heat flux following exposure (Figure 5). Exposure duration appeared to influence the magnitude of the bias in transferred energy (Figure 4).

4 | DISCUSSION

Manikin sensors must perform consistently in order for the ISO 13506 standard to be reproducible. For the first time, a range of existing manikin sensors (from nine laboratories and encompassing three sensor families) were evaluated on the same instrumented test cylinder during short duration heat and flame engulfment tests similar to those defined by ISO 13506-1:2017. Prior to testing, all manikin sensors were calibrated according to ISO 13506-1:2017 using a radiant only heat source at the laboratory of sensor origin. The main finding of this work was that the performance of the manikin sensors varied when subjected to a mixed-mode heat source (approximately 50:50 radiant to convective heat) representative of the manikin exposure calibration conditions of ISO 13506-1. Calibration tests

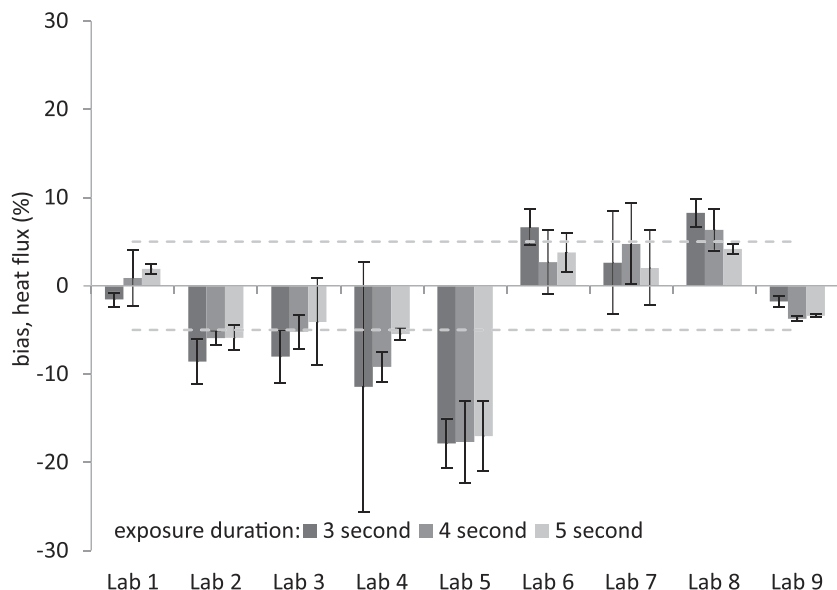


FIGURE 3 Manikin sensor bias in heat flux for each burn duration. Error bars: inter-test standard deviation. Note for Labs 4 and 5 a single sensor has been excluded from the analysis

TABLE 5 Post-exposure offset for each exposure duration

Lab	Mean offset \pm SD (kW/m^2)		
	3 s	4 s	5 s
1	0.0 ± 0.0	-0.1 ± 0.1	-0.1 ± 0.0
2	0.1 ± 0.0	0.1 ± 0.0	0.1 ± 0.1
3	0.1 ± 0.0	0.2 ± 0.0	0.1 ± 0.0
4 ^a	-0.1 ± 0.0	-0.2 ± 0.0	-0.4 ± 0.1
5 ^a	0.8 ± 0.0	1.1 ± 0.0	1.4 ± 0.0
6	0.5 ± 0.1	0.6 ± 0.1	0.9 ± 0.0
7	0.3 ± 0.0	0.4 ± 0.0	0.3 ± 0.0
8	-5.1 ± 0.1	-7.1 ± 0.2	-8.7 ± 0.2
9	-3.7 ± 0.1	-5.3 ± 0.1	-6.7 ± 0.2

^aFor laboratories 4 and 5 a single sensor has been excluded from analysis (Appendix A2)

(nude exposures) are used to set the incident heat flux for the subsequent garment tests and are therefore critical in ensuring consistency within and between laboratories. Below we discuss, first,

the performance of the manikin sensor technologies in response to mixed-mode heat, second, the reasons for the differences in manikin sensor performance (heat loss due to sensor design and sensitivity to convective heat) and, third, the stability and repeatability of the fire produced during short duration heat and flame engulfment tests. Based on this work several recommendations are made that would improve the reproducibility of the standard.

4.1 | Comparing the performance of manikin sensor technologies

This work has quantified the differences which exist among the manikin sensor technologies when such sensors are exposed to a mixed-mode heat source representative of ISO 13506-1. These differences include instances of relevant heat flux biases when compared to traceable, commercial THF sensors (>5%), post-exposure offsets in heat flux, and combinations thereof. Of the three manikin sensor families investigated (buried thermocouple sensors,

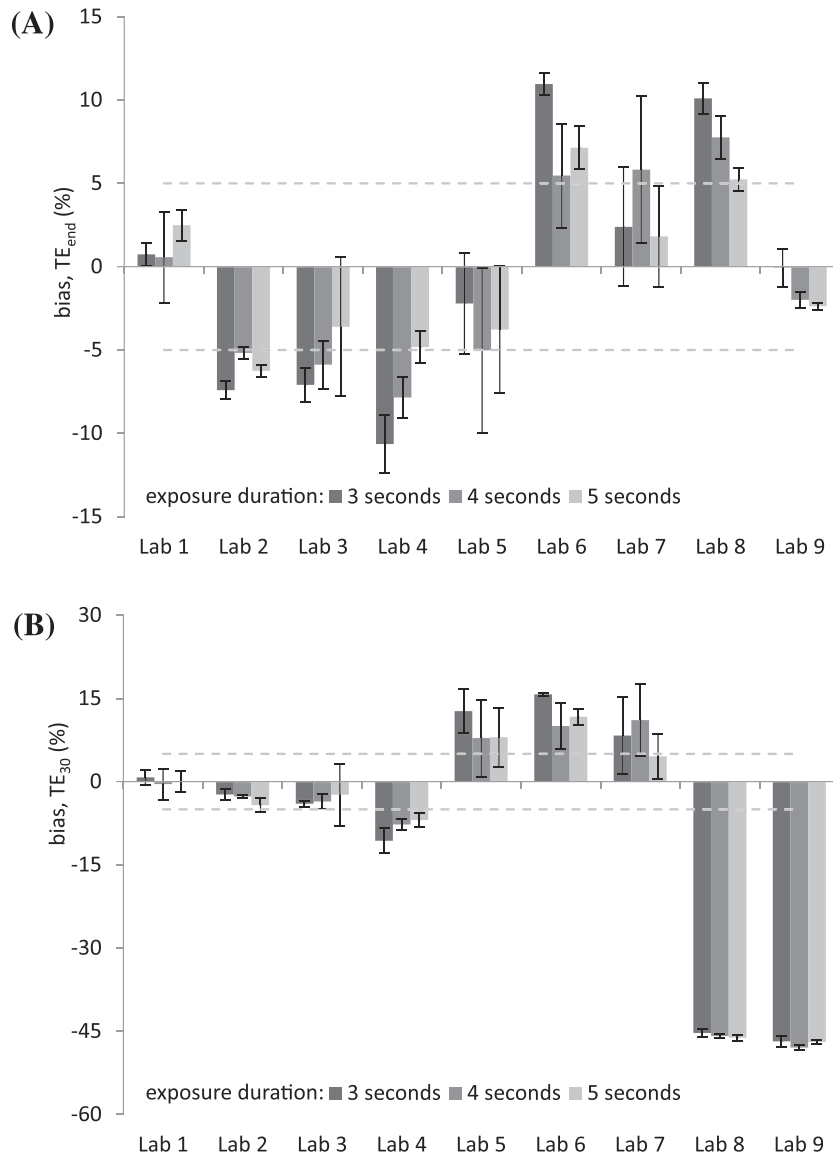


FIGURE 4 The bias in transferred energy by laboratory for each exposure duration at A, TE_{end} and B, at TE_{30} . Note for Labs 4 and 5 a single sensor has been excluded from the analysis

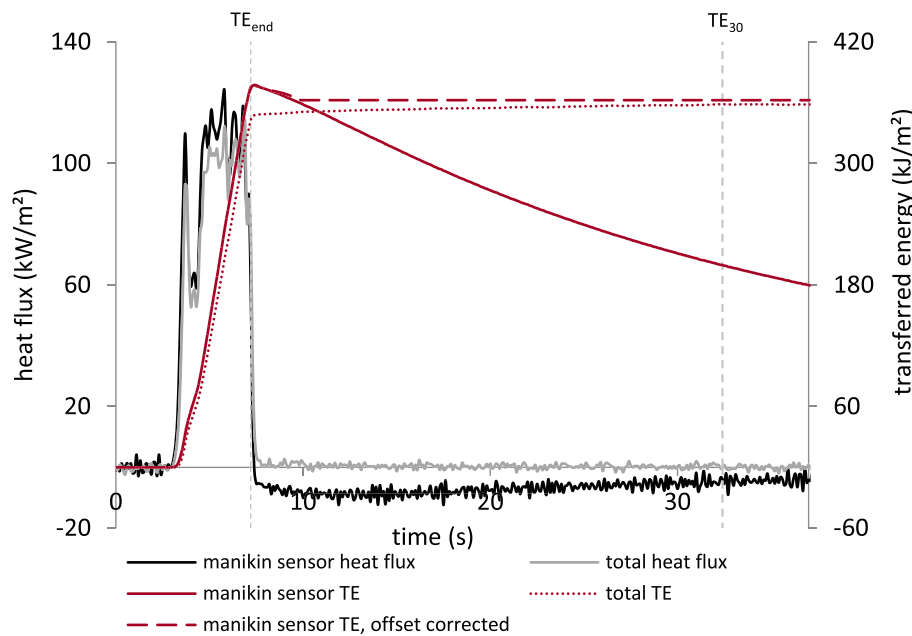


FIGURE 5 An example of the heat flux and transferred energy a manikin sensor in comparison to the THF, illustrating the influence of offset, if uncorrected, on TE (Lab 8, 4-second exposure). The influence of clipping the negative offset values on the TE, as permitted by ISO13506-1:2017, is also demonstrated

copper-based sensors, and surface-mounted thermocouple sensors), there was not a single family that performed considerably better than the others in all aspects.

The sensor response to exposure can be divided into four distinct phases based on the heat flux profile over time: 1) transient increase, 2) pseudo-steady state, 3) transient decrease, and 4) post-exposure. For all sensor types, it was possible to implement a single definition of pseudo-steady state. With the current definition, a 3-second exposure had a pseudo-steady state duration of only ~1 s. Accordingly, the suitability of conducting manikin exposure calibration and garment tests with a 3-second exposure duration needs to be reconsidered (as discussed below, short exposure durations also had negative implications on sensor bias and heat source stability).

During transient increase (phase 1) the fire impinges on the test apparatus. An increase in the sensor surface temperature results in a steep increase in heat flux. The heat flux then invariably drops before increasing again prior to the period of pseudo-steady state. The exact cause of this drop in heat flux is unknown but may be due to changes in the availability of oxygen at the surface of the test cylinder or instability in the gas pressure.

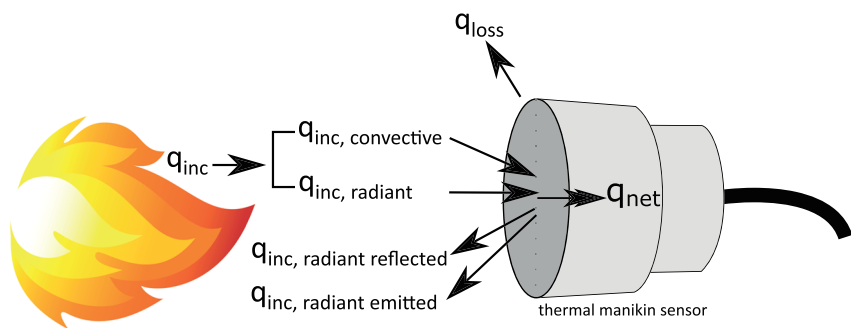
Over the duration of pseudo-steady state (phase 2), manikin sensors from five of the nine participating laboratories showed considerable bias in heat flux (greater than $\pm 5\%$) in relation to the THF for the 4-second exposures. Of those five sensor types, four underestimated heat flux and one overestimated heat flux. Exposure duration appeared to influence the manikin sensor bias, with greater bias typically observed for shorter exposure durations. The practical implication of sensor bias is that a given laboratory will then adjust the heat source (for example by altering gas pressure or torch distances) in order to reach an ostensible incident heat flux of $84 \text{ kW/m}^2 \pm 5\%$ required during manikin exposure calibration.¹ This deviation in the heat source at calibration is then applied to the

garment exposure which could account for the large variation in garment destruction, transferred energy, and burn risk (ISO 13506-2) observed in the ISO 13506 2016 round robin.⁵

A small negative offset in heat flux was recorded by the THF sensors (-0.2 kW/m^2), indicating that energy is transferred from the sensor surface back to the environment post exposure. It is however problematic that some sensor technologies showed considerably more, or less, offset than the THF sensors. The manikin sensors from two laboratories (Labs 8 and 9) had a negative offset in heat flux post-exposure (phase 4) greater than $\pm 5.0 \text{ kW/m}^2$, both laboratories used copper-based sensors. Laboratory 7 (also copper-based sensors) have implemented a correction for offset into their calibration algorithm (Table 3) and have an offset less than $\pm 0.5 \text{ kW/m}^2$. Laboratories 8 and 9 reported that, while offset corrections were not made to this data, as requested, they typically would make corrections during standard tests. The sensors from Labs 5 and 6 had smaller positive offsets (between $0.5\text{--}1.0 \text{ kW/m}^2$), for these labs corrections are not made during standard testing (email communication July 28, 2018). The ISO 13506-1:2017 standard identifies two methods to correct for offset. However, it is important to understand the cause of the offset (for example sensor design, calibration procedure, and method for calculating heat flux) in order to appropriately correct the data without losing real data in the process. Offset, if not appropriately corrected for, has a considerable impact on transferred energy over time. The implications of nude exposure offset on the results under fabrics are currently unknown.

Transferred energy is a useful measure as it allows the entire burn, or phases of interest, to be quantified.²⁴ However, for transferred energy to be a comparable measure, the sensor technologies must respond equivalently to the incident heat flux. How quickly each sensor responds to the transient changes in incident heat flux may also impact the transferred energy at a given time point. While the quantification of response time is beyond the

FIGURE 6 Energy transfer to and from the sensor during a nude exposure



scope of this work, visual analysis of the heat flux curves (Appendix 1) shows that some labs (particularly Lab 5) have a delayed response in phases 1 and 3. A positive bias in heat flux generally resulted in a positive bias in transferred energy at TE_{end} and TE_{30} , and vice versa, the exceptions being Labs 5 and 8 where the bias at TE_{30} was impacted by the post-exposure offset (Figures 3–5). Corrections for offset, as permitted by the ISO 13506-1 standard, would mitigate such deviations in TE_{30} (Figure 5). ISO13506-1:2017 does not currently restrict the transferred energy attained during a nude exposure, rather this is controlled by the heat flux during pseudo-steady state ($84 \text{ kW/m}^2 \pm 5\%$). However, given that transferred energy is a reported outcome for garment exposures, it is critical that transferred energy is comparable across the manikin sensors.

In the current work, the post-processing of the heat flux data was not controlled and thus varied between laboratories as it currently would with standard testing. Post-processing appears to have influenced the magnitude of the peaks and troughs over the duration of the exposure (Appendix 1). The impact of specific data processing tools on the transferred energy and burn risk is of importance but is beyond the scope of this work. The impact of sampling rate (for example, potential response time mismatches) also requires further investigation.

In addition to the variation between manikin sensor families, variation was observed within the families of sensor technologies, that is, within the buried thermocouple sensors and within copper-based sensors. Such variation may be due to differences in 1) sensor design (e.g., sensor size, composition, and structure of the guard), 2) the method of calibration (e.g., definition of steady state, exposure duration, heat source, heat flux range, and the position of the reference sensor relative to the manikin sensor; Table 2), and 3) the conversion from temperature to heat flux. Only a single laboratory used the surface-mounted thermocouple sensor and thus the variation within this manikin sensor family could not be assessed.

4.2 | Understanding the differences in manikin sensor performance

The net heat flux (q_{net}) measured by the manikin sensors during exposure to a mixed-mode heat source has been shown to be dependent on the manikin sensor used. Given the variation in manikin sensor performance, it can no longer be assumed, as the ISO 13506

standard has historically done, that q_{net} is equal to the incident energy (q_{inc}). The relationship between q_{inc} (in this work a combination of radiant and convective energy) and q_{net} is depicted by Figure 6 and Equation (Eq 2). The differences in each sensor technology's performance may primarily be attributed to mechanisms of q_{loss} , including the sensitivity of the sensor to convective heat transfer. q_{loss} is dependent on sensor design and composition and therefore varies between the sensor technologies. q_{loss} encompasses the unintentional heat transfer to design components such as thermal guards, holders/mounts, pins, and adhesives. The sensitivity of the manikin sensors to convective heat transfer cannot currently be accounted for when the manikin sensors are calibrated using only a radiant heat source.

$$q_{net} = q_{inc,convective} + q_{inc,radiant} - q_{radiant,reflected} - q_{radiant,emitted} - q_{losses} \quad (\text{Eq2})$$

Each manikin sensor technology has its drawbacks. The copper-based sensors, for example, have the potential for heat loss at the boundaries to the guard or supporting structure.⁹ In contrast, the placement of the thermocouple and the material properties of the buried thermocouple sensors means there is minimal heat loss at the boundaries. However, the buried thermocouple sensors therefore rely on the accurate calculation of surface temperature based on the inverse heat equation.^{6,25} The surface-mounted thermocouple sensors use an adhesive to affix the thermocouple to the sensor surface which creates a physical perturbation on the surface and the possibility of loss due to the insulative effect of the adhesive.^{26,27}

The contribution of convective heat transfer to the manikin sensors is dependent on 1) the convective heat transfer coefficient, which is a function of fluid velocity and physical properties, 2) sensor surface area and sensor properties (i.e. shape, orientation, and surface roughness, and heat capacity of the sensing element if temperature dependent), and 3) the difference in temperature between the surface and the approaching fluid, in this instance, $T_{flame} - T_{surface}$ (Newton's law of cooling)^{3,28,29}. As the surface temperature of the manikin sensor increases, the convective heat transfer to the sensor ($q_{convective}$) decreases and the radiant emitted ($q_{radiant,emitted}$) increases

³Newton's law of cooling: $q = h.A.\Delta T$, where: q = heat transfer to the sensors by convection, h = the convection heat transfer coefficient, A = the surface area of the sensor, ΔT = the difference in temperature between the sensor surface and the approaching fluid.

(Stefan–Boltzmann law¹³). The magnitude of the increase in sensor surface temperature will vary between sensor types due to differences in sensor design and composition. As demonstrated in Table 4, the thermal properties for each sensor type vary considerably.³⁰ Heat will move quickly through the material and away from the sensor surface in sensors with a high thermal diffusivity. Of the sensors investigated copper has the highest thermal diffusivity. The buried thermocouple and surface-mounted thermocouple sensors are constructed from materials that more closely resemble the thermal properties of human skin. An increase in exposure duration from 3 to 5 seconds results in an increase in the surface temperature of the manikin sensors, and thus a decrease in the amount of convective heat transfer. The decrease in convective heat transfer may account for the decrease in sensor bias typically seen at 5 seconds when compared to that at 3 seconds.

The energy measured at the surface of the cylinder during pseudo-steady state was approximately 50% radiant heat and 50% convective heat. It is recommended that this partitioning is adopted by all labs in the calculation of incident heat flux. The partitioning of energy during pseudo-steady state was not influenced by exposure duration. Here, the surface temperature, and thus the convective heat transfer, of the water cooled THF sensors remains fairly constant. For the manikin sensors, which are not water cooled, the convective fraction at the sensor surface is expected to be lower than that recorded by the THF sensors.¹² Between tests, the partitioning of energy was observed to be highly variable (inter-test CV for 4-second exposures was 12%), such variability is thought to be due to the stochastic nature of the convective energy. The ratio of convective to radiant heat is expected to vary further within and between ISO 13506 manikin test systems. Test parameters such as torch type, torch configuration (e.g., distance, angle, and pressure), fuel composition, sensor position and orientation, manikin geometry, and chamber size may influence fire temperature and flame velocity, and thus convective heat transfer.

The differences in manikin sensor performance are an unacceptable source of variation which is not adequately addressed by the ISO 13506-1:2017 manikin standard. There are two options that would decrease the current variation. Ideally, a single manikin sensor technology would be defined by the standard and used by all laboratories. While the selected sensor may not accurately measure the total heat flux, the same errors would be made across all laboratories producing comparable results.¹¹ The selection of the single manikin sensor would need to consider sensor performance, repeatability, cost, availability, and durability.⁶ Given recent advances in heat flux sensor technology the selection of a single sensor technology should not be restricted to those currently used by the laboratories. Realistically, a move to a single sensor technology may not be a practical solution for the laboratories given the costs involved. The second option is to standardise a transparent model for each sensor technology to ensure that sensor heat losses, including

the sensitivity to convective energy and heat loss due to sensor design, are accounted for. One negative implication of modelling each manikin sensor technology is the considerable increase in the measurement error.

Both the manikin and THF sensors used within this work were calibrated using primarily radiant heat sources, creating a discrepancy between the calibration environment and the application environment. The difficulties associated with the calibration of heat flux sensors to measure total heat flux in mixed-mode environments have been acknowledged in the scientific literature.^{11,13,26,27,31} In 1999 NIST reported a method for calibrating against convective heat, and yet twenty years later it remains difficult to acquire sensors calibrated for both radiation and convection. Tighter regulation of the sensor calibration procedure by future ISO 13506 standards could reduce the variation in manikin sensor performance, both between and within laboratories. Areas for immediate consideration include: 1) the defined heat source—preferably a uniform radiant only heat source where the spectral content of the radiant energy is closer to that encountered during short duration heat and flame engulfment tests,³² 2) data collection, e.g. defining the duration of exposure and further limiting THF metres that are compliant, and 3) data evaluation e.g. further defining pseudo-steady state and post-processing of data.

4.3 | Stability and repeatability of the heat source

The fire generated during short duration heat and flame engulfment tests is not a stable source of energy. Over the duration of pseudo-steady state, the mean standard deviation for each THF sensor was 11 kW/m² (CV of 13%). Visual observations confirm the temporally chaotic nature of the heat generated by the propane flames, where the flames can be seen moving on and off the sensor surface during the exposure. Variation was also observed in the heat flux distribution across the surface of the cylinder (intra-test CV of 4.4%) and in the heat flux between tests (inter-tests CV of 8.7%). Exposure duration appeared to influence the intra-test variation, with greater variation observed for 3-second exposures than for 4- and 5-second exposures. The instability, intra- and inter-test variation suggests that the propane torches are not an ideal heat source for routine calibration of individual manikin sensors. However, in order to accurately model sensor response, it is crucial that manikin sensor technologies are validated with a mixed-mode heat source that is representative of those in manikin tests.

The repeated measurement of the heat flux during exposure to short duration heat and flame engulfment has provided practical insight into the levels of repeatability attainable using such a heat source. In this work, the inter-test repeatability was assessed with a number of constant test parameters, for example, sensor type (externally calibrated THF sensors), the definition of pseudo-steady state, collection frequency, torch type and configuration, sensor positioning and orientation, gas concentration and pressure, test chamber volume. These parameters, each with their own measurement error, currently vary between manikin systems.^{5,30}

#. Stefan–Boltzmann law states that the black-body radiation energy emitted by an object is proportional to the temperature of the object raised to the fourth power.

5 | CONCLUSIONS

There is considerable variation in the performance of existing manikin sensors when exposed to short duration heat and flame engulfment, despite all tested sensors conforming to ISO 13506-1:2017. Of the manikin sensors evaluated, there is not a single sensor technology which performs ideally in all respects. Some manikin sensors demonstrated a relevant bias in heat flux when compared to traceable, commercial THF sensors (>5%), whereas other sensors had post-exposure offsets, or a combination thereof. To attain a reproducible standard, the variations in manikin sensor performance must be addressed by either restricting ISO13506 to a single sensor technology or by better modelling each sensor technology to include the influence of convective heat transfer and sensor heat losses due to sensor design. While the continual modification of the test standard is not ideal for the end user as it impacts the continuity of results, it is essential that improvements be made in order to achieve reproducible results across the laboratories and ensure consumer confidence.

All of the sensors tested followed a similar profile in net heat flux over time, which could be divided into four distinct phases, 1) transient increase, 2) pseudo-steady state, 3) transient decrease, and 4) post-exposure. Therefore, it was possible to implement a single definition of pseudo-steady state for all manikin sensors. The partitioning of radiant to convective heat during the pseudo steady-state period of the short duration heat and flame engulfment tests was determined to be approximately 50:50, but highly variable. The heat source instability and the intra- and inter-test variability in the total heat flux suggest that the test apparatus (cylinder and torches) may not be ideal for the routine calibration of sensors using a mixed-mode heat source. However, it is evident that the calibration process as currently defined in the ISO 13506-1 standard (8-30 kW/m², radiant only heat source) requires reform. The repeated measurement of the heat flux has also given valuable insight into the levels of repeatability attainable from the heat source defined by ISO 13506-1. Further work is required to understand the impact of, among others, manikin sensor response times, data processing (filtering and smoothing), the performance of sensors under garments where the total heat flux is lower and the modes of heat transfer vary,³³ and burner configuration.

ACKNOWLEDGEMENTS

The authors would like to acknowledge the valuable contribution of the US Army Natick Soldier RD&E Center engineers for the fabrication of the test apparatus and Rolf Stämpfli, Empa, for his technical assistance during data evaluation.

We are also grateful to those who continue to work toward the improvement of thermal manikin standards, in addition to the listed authors Eric van Wely, Dave Matthews, and personnel from the University of Alberta, Aitex, BTTG, CTT Group, DuPont, Dankook University, Donghua University, Empa, US Army Natick, North Carolina State University, Teijin, and Thermetrics.

The following scientists have endorsed this paper and have provided suggestions or comments to the test procedure or manuscript: Doug Dale (University of Alberta) and Eric van Wely (DuPont International Operations, Switzerland).

FUNDING AND DISCLAIMERS

This research received no specific grant from any funding agency in the public, commercial, or not-for-profit sectors. The authors declare that there is no conflict of interest.

ORCID

Shelley Kemp  <https://orcid.org/0000-0002-2812-9020>

REFERENCES

- ISO 13506-1. *Protective Clothing against Heat and Flame – Part 1: Test Method for Complete Garments – Measurement of Transferred Energy Using an Instrumented Manikin*. Geneva, Switzerland: International Organization for Standardization; 2017.
- ISO 13506-2. *Protective Clothing against Heat and Flame – Part 2: Skin Burn Injury Prediction – Calculation Requirements and Test Cases*. Geneva, Switzerland: International Organization for Standardization; 2017.
- ISO 14934-2. *Fire Tests – Calibration and Use of Heat Flux Meters – Part 2: Primary Calibration Methods*. Geneva, Switzerland: International Organization for Standardization; 2013.
- Stoll AM, Greene LC. Relationship between pain and tissue damage due to thermal radiation. *J Appl Physiol*. 1959;14(3):373-382. <https://doi.org/10.1152/jappl.1959.14.3.373>
- Camenzind MA, Kemp SE, van Wely E. N108 Final Draft RR ISO 13506-1 Non Confidential. Round Robin Testing Using ISO DIS 13506-1 on Thermal Manikin Systems, Sensor and Manikin Calibration, Standard Overalls and Structural Firefighter Testing. Available from secretariat of ISO/TC 94/SC 13/WG 2; 2016.
- Barker RLR, Hamouda H, Shalev I, Johnson J. *Review and Evaluation of Thermal Sensors for Use in Testing Firefighters Protective Clothing - NIST GCR 99-773*. National Institute of Standards and Technology: Gaithersburg; 1999.
- Mandal S, Song G. Thermal sensors for performance evaluation of protective clothing against heat and fire: a review. *Text Res J*. 2015; 85(1):101-112. <https://doi.org/10.1177/0040517514542864>
- ISO 9151. *Protective Clothing against Heat and Flame - Determination of Heat Transmission on Exposure to Flame*. Geneva, Switzerland: International Organization for Standardization; 1995.
- Hightower TM, Olivares RA, Philippidis D. Thermal capacitance (slug) calorimeter theory including heat losses and other decaying processes. NASA. 2008;TM-2008-21(September).
- ISO 9162. *Petroleum Products – Fuels (Class F) – Liquefied Petroleum Gases – Specifications*. Geneva, Switzerland: International Organization for Standardization; 2013.
- Wickström U, Wetterlund I. Total heat flux cannot be measured. In: *Interflam, International Conference Fire Science and Engineering*; 2004: 269-276.
- Pullins CA, Diller TE. Direct Measurement of Hot-Wall Heat Flux. *J Thermophys Heat Transf*. 2012;26(3):430-438. <https://doi.org/10.2514/1.59246>
- Lam C, Weckman E. Steady-state heat flux measurements in radiative and mixed radiative-convective environments. *Fire Mater*. 2009;33: 303-321. <https://doi.org/10.1002/fam>
- Song G, Mandal S, Rossi R. *Thermal Protective Clothing for Firefighters*. Amsterdam: Woodhead Publishing; 2017 10.1016/B978-0-08-101285-7.00005-8.

15. Steketee J. Spectral emissivity of skin and pericardium. *Phys Med Biol.* 1973;18(5):686-694. <https://doi.org/10.1088/0031-9155/18/5/307>
16. ISO 6942. *Protective Clothing – Protection against Heat and Fire – Method of Test: Evaluation of Materials and Material Assemblies When Exposed to a Source of Radiant Heat.* Geneva, Switzerland: International Organization for Standardization; 2002.
17. ASTM F1939-15. *Standard Test Method for Radiant Heat Resistance of Flame Resistant Clothing Materials with Continuous Heating.* ASTM International: West Conshohocken, PA; 2015 10.1520/F1939-15.
18. Raynaud M, Bransier J. A new finite-difference method for the nonlinear inverse heat conduction problem. *Numer Heat Transf Part A Appl.* 1986;9(1):27-42. <https://doi.org/10.1080/10407788608913463>
19. Crown E, Dale J. *Evaluation of Flash Fire Protective Clothing Using an Instrumented Mannequin; Report Prepared for Alberta Occupational Health and Safety Heritage Grant Program.* Alberta, Canada: Protective Clothing and Equipment Research Facility, University of Alberta; 1992.
20. Torvi DA, Dale JD. A finite element model of skin subjected to a flash fire. *J Biomech Eng.* 1994;116(3):250-255. <https://doi.org/10.1115/1.2895727>
21. Song G, Barker R, Grimes DR, Thompson D. Comparison of methods used to predict the burn injuries in tests of thermal protective fabrics. *J ASTM Int.* 2005;2(2):1-11. <https://doi.org/10.1089/adt.2005.3.309>
22. Ryoden Kaseo. Data Sheet No. 558885: General property of MIOLEX. 2018.
23. Mills KC. Cu Pure Copper. In: Mills KC, ed. *Recommended Values of Thermophysical Properties for Selected Commercial Alloys.* Cambridge, England: Woodhead Publishing Limited; 2002:89-97 10.1533/9781845690144.89.
24. Rossi RM, Schmid M, Camenzind MA. Thermal energy transfer through heat protective clothing during a flame engulfment test. *Text Res J.* 2014;84(13):1451-1460. <https://doi.org/10.1177/0040517514521115>
25. Berntsson F. *Numerical Solution of an Inverse Heat Conduction Problem.* Sweden: Linköpings Universitet; 1998 <http://hdl.handle.net/2060/19760010238>.
26. Diller TE. Heat flux measurement. In: Kutz M, ed. *Handbook of Measurement in Science and Engineering.* New York, USA: John Wiley & Sons; 2013:629-659 10.1016/b978-075065080-9/50012-5.
27. Holmberg D, Steckler K, Womeldorf C, Grosshandler W. Facility for calibrating heat flux sensors in a convective environment. *Proc ASME Heat Transf Div.* 1997;HTD-3:165-171.
28. Peterson GP. Heat transfer fundamentals. In: Kutz M, ed. *Eshbach's Handbook of Engineering Fundamentals.* Fifth Edit ed. Hoboken, New Jersey: John Wiley & Sons, Inc.; 2009:818-869 10. 1002/9780470432754.ch15.
29. Huynh T. Fundamentals of thermal sensors. In: Jha CM, ed. *Thermal Sensors: Principles and Applications for Semiconductor Industries.* New York, USA: Springer; 2015:5-42 10.1007/b136378_3.
30. Camenzind MA, Dale DJ, Rossi RM. Manikin test for flame engulfment evaluation of protective clothing: Historical review and development of a new ISO standard. *Fire Mater.* 2007;31(5):285-295. <https://doi.org/10.1002/fam.938>
31. Pitts WM, De Ris JL, Wetterlund I. Round Robin Study of Total Heat Flux Gauge Calibration at Fire Laboratories, NIST Special Publication 1031. 2004.
32. DeWerth DW. *A Study of Infra-Red Energy Generated by Radiant Gas Burners.* U.S.A: American Gas Association, Inc.; 1962.
33. Kim IY, Lee C, Corner BD, Li P. Investigation of air gaps entrapped in protective clothing systems. *Fire Mater.* 2002;26(3):121-126. <https://doi.org/10.1002/fam.790>

How to cite this article: Kemp S, Proulx G, Auerbach M, Grady M, Parry R, Camenzind M. Thermal sensor performance and fire characterisation during short duration engulfment tests. *Fire and Materials.* 2020;1-18. <https://doi.org/10.1002/fam.2784>

APPENDIX 1

Net heat flux profiles over time

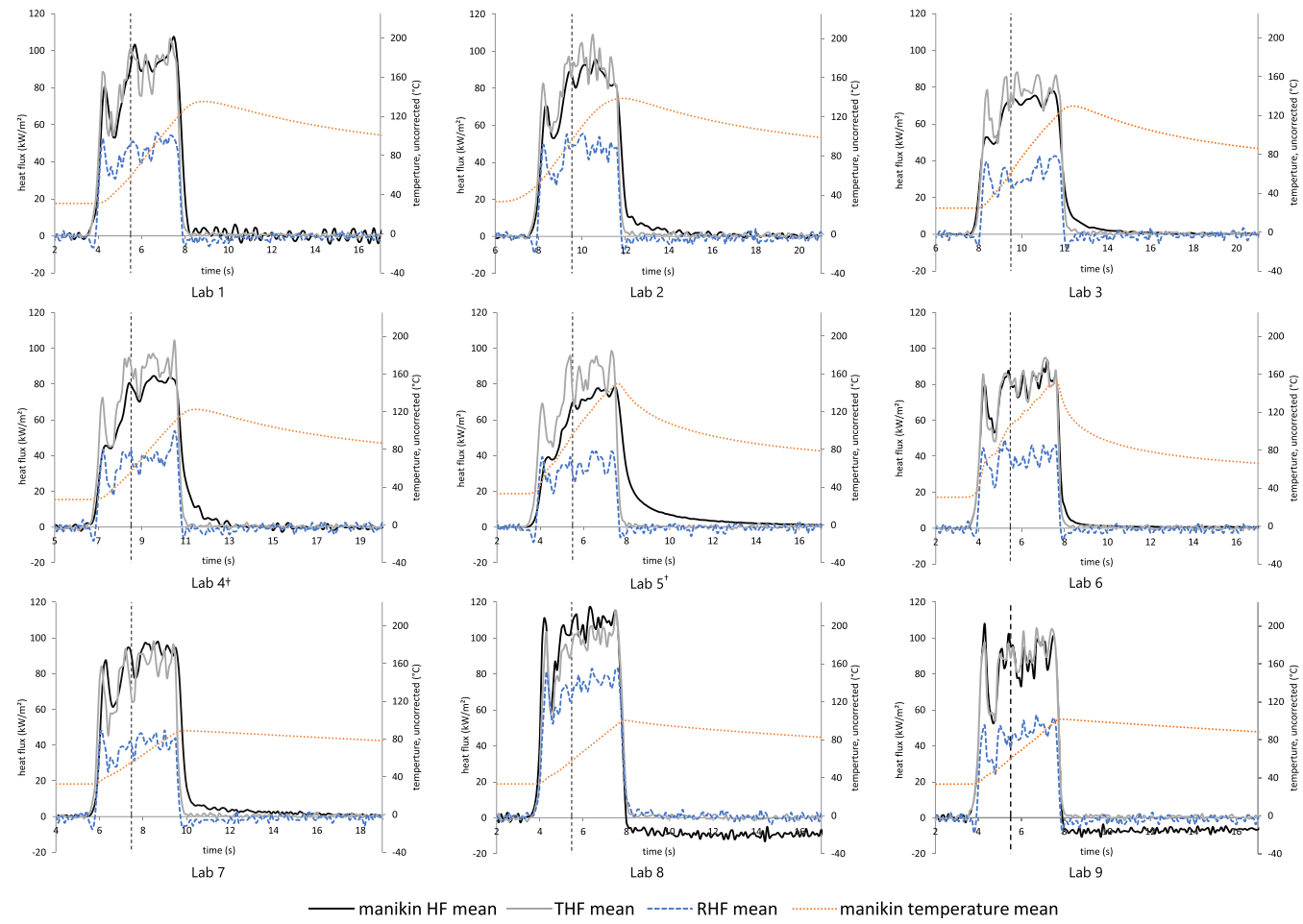


FIGURE A1.1 Typical examples of the net heat flux over time for each sensor type: RHF ($n=1$), THF mean ($n=4$) and manikin sensor mean ($n=3$), for a 4-second exposure. The mean manikin temperature ($n=3$) is displayed on the secondary axis, this is the raw data output from the thermocouple (either at the surface or buried within the sensor) and is thus uncalibrated and uncorrected.[†]For laboratories 4 and 5 a single defective sensor was excluded from analysis, for both heat flux and temperature ($n=2$, Appendix 2)

APPENDIX 2

Excluded manikin sensors

TABLE A2.1 The intra-test variation between the three manikin sensors expressed as a mean of the three replicate exposures

Lab	Mean standard deviation [kW/m ²]		
	3-s exposure	4-s exposure	5-s exposure
1	8.6	9.1	6.9
2	2.6	2.3	4.5
3	5.4	5.3	3.2
4	42 [4.3]	44 [3.9]	28 [4.2]
5	45 [23.7]	44 [20.7]	34 [18.3]
6	3.8	3.2	1.8
7	4.0	9.0	8.0
8	8.6	9.1	6.9
9	5.2	3.6	4.9
THF sensor	4.6	3.6	3.4

Note. the value in brackets is the SD when a single defective manikin sensor was excluded from the analysis.

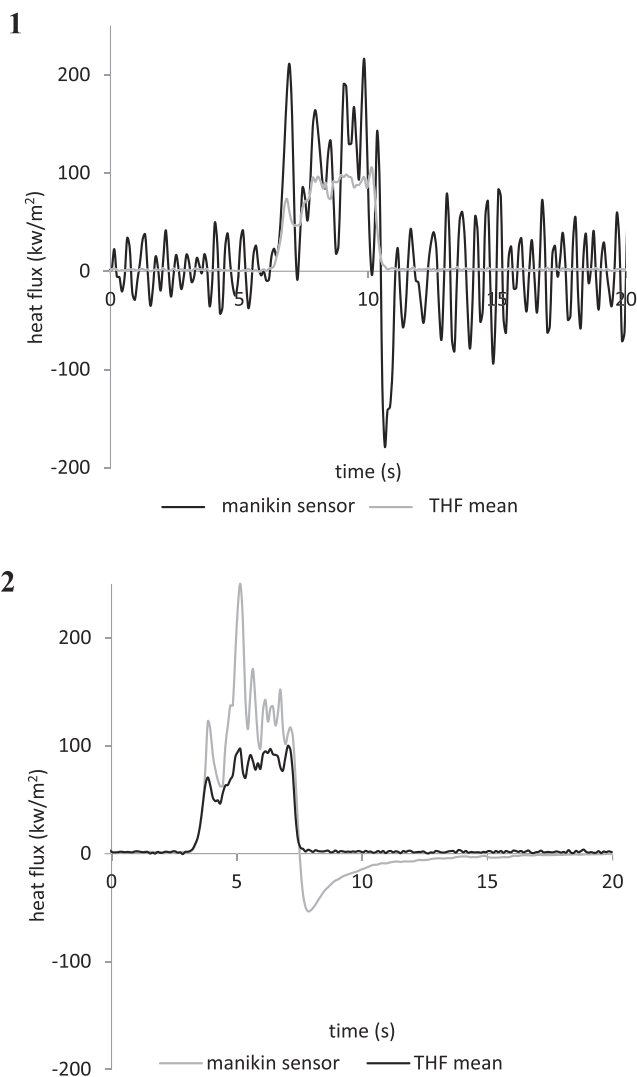


FIGURE A2.1 A typical example of the heat flux profile from the excluded manikin sensors compared to the mean THF for the same exposure, 1) Lab 4, 4-second exposure, manikin sensor, 2) Lab 5, 4-second exposure, manikin sensor 2